PNAS

Supporting Information for

Propagating spatio-temporal activity patterns across macaque motor cortex carry kinematic information

Wei Liang[1,2], Karthikeyan Balasubramanian[2], Vasileios Papadourakis[2], Nicholas G. Hatsopoulos[1,2,*]

[1] Committee on Computational Neuroscience, University of Chicago, Chicago, IL, USA

[2] Organismal Biology and Anatomy, University of Chicago, Chicago, IL, USA

* Nicholas G. Hatsopoulos

Email: nicho@uchicago.edu

This PDF file includes:

Text

Figures S1 to S8

Tables S1 to S6

Propagation patterns encoded for not only the launch angle but also later kinematics

In the main text, we established that propagation patterns encoded for launch velocities. Here we probe whether the patterns also contained information regarding later parts of the trajectory, controlling for the autocorrelation in the velocities.

We used launch velocities (x velocity and y velocity at movement onset) to predict velocities at later time points (from 20 to 400ms in steps of 20 ms, one model for each time point), and compared its performance with using both launch velocities and high-gamma spatial variables to predict velocities. For monkey Bx, there was no significant difference in the performance including or excluding high-gamma spatial variables on top of launch velocities, because he had been making relatively straight trajectories and there was a strong autocorrelation in the velocities (Supplementary Figure 6a, top panel). Thus for Bx, we could not rule out the fact that all the prediction for later velocities came from prediction of launch velocities. However, for monkey Ls, there were two targets where he made bent trajectories (90° and 135° targets, mean trajectories shown in the inset of Supplementary Figure 6b, top panel), in which cases high-gamma spatial variables provided significant additional prediction power on top of launch velocities, precisely at those time when he was transitioning from moving forward to moving to the left in the curved trajectory (several time points from 80~180ms; stars indicate that propagation parameters can predict kinematics significantly better than using launch velocities at the time points from single-tailed Wilcoxon test, Bonferroni-corrected for multiple comparisons). This improved prediction was primarily driven by the propagation direction (orange trace in Supplementary Figure 6b, bottom panel) and planar fitness (green trace in Supplementary Figure 6b, bottom panel).

Granted that this center-out task was not the best to detect such encoding for later parts of the trajectory, we still found that high-gamma spatial patterns possessed such information at least when velocities were less autocorrelated, in the form of planned curved trajectories. We plan to study this phenomenon more thoroughly with other movement tasks which included multiple submovements or ongoing corrections that are either planned or unplanned, to establish this concretely.

Analyses of 100-200Hz high-gamma band

Here we examined an alternative definition of the high-gamma band, which is a lower frequency range from 100-200Hz. We performed all the analyses we did with the 200-400Hz band.

For Bx, the mean (standard deviation) of the median amplification times was -111.9ms (68.8ms) for the lateral array and -82.5ms (92.5ms) for the medial array. For Ls, the mean median amplification time was -82.8ms (53.2ms) for the lateral array and -60.1ms (71.0ms) for the medial array. These amplification times were similar to results from 200-400Hz within variation.

Next, we computed the propagation patterns based on 100-200Hz signal. For the lateral arrays, 1269 out of 2435 trials (52%) exhibited significant planar propagation patterns for Bx and 687 out of 1079 trials (64%) for Ls exhibited significant planar propagation patterns. For the medial arrays, 599 out of 2435 trials (25%) exhibited significant planar propagation patterns for Bx, and for Ls 449 out of 1079 trials (42%). These ratios of significant propagations were largely similar to the results from 200-400Hz. Propagation directions were significantly different across target directions in both arrays for both monkeys (lateral array: $p=0.003$ for Bx, $p<0.001$ for Ls; medial array: $p=0.017$ for Bx, $p<0.001$ for Ls, non-parametric test for common median for multiple groups

of angles). Nevertheless, there was often larger variance in propagation direction for a given movement direction (sometimes bimodal), resulting in lower mean vector lengths (i.e. lower r values in Supplementary Table 3, 4, 5 and 6).

Like the 200-400Hz results, the propagation in the two arrays were related. The propagation speed in the medial array was correlated with the propagation speed in the lateral array for both monkeys (for Bx, Pearson correlation coefficient $r= 0.682$, $p<0.001$, $n=402$; for Ls, $r=0.581$, $p<0.001$, $n=277$). Also, the median amplification time in the medial array was correlated with the median amplification time in the lateral array for both monkeys (for Bx, Pearson correlation coefficient $r= 0.783$, $p<0.001$, $n=401$; for Ls, $r=0.775$, $p<0.001$, $n=277$).

All the kinematic decoding conclusions qualitatively held as well, though all the decoding performances were weaker than using their 200-400Hz counterparts. The highest kinematic prediction performance using first order spatial parameters of 100-200Hz was a composite R^2 of 0.127 instead of 0.427 from 200-400Hz for Bx (a 70% drop of performance) and a composite R^2 of 0.151 instead of 0.268 from 200-400Hz for Ls (a 44% drop of performance). The prediction performance using both envelope amplitudes and spatial variables (1^{st} and 2^{nd} order) were also lower than using 200-400Hz, with a ~0.38 decrease in composite R^2 for Bx (a 50% drop of performance) and a ~0.15 decrease for Ls (a 23% drop of performance).

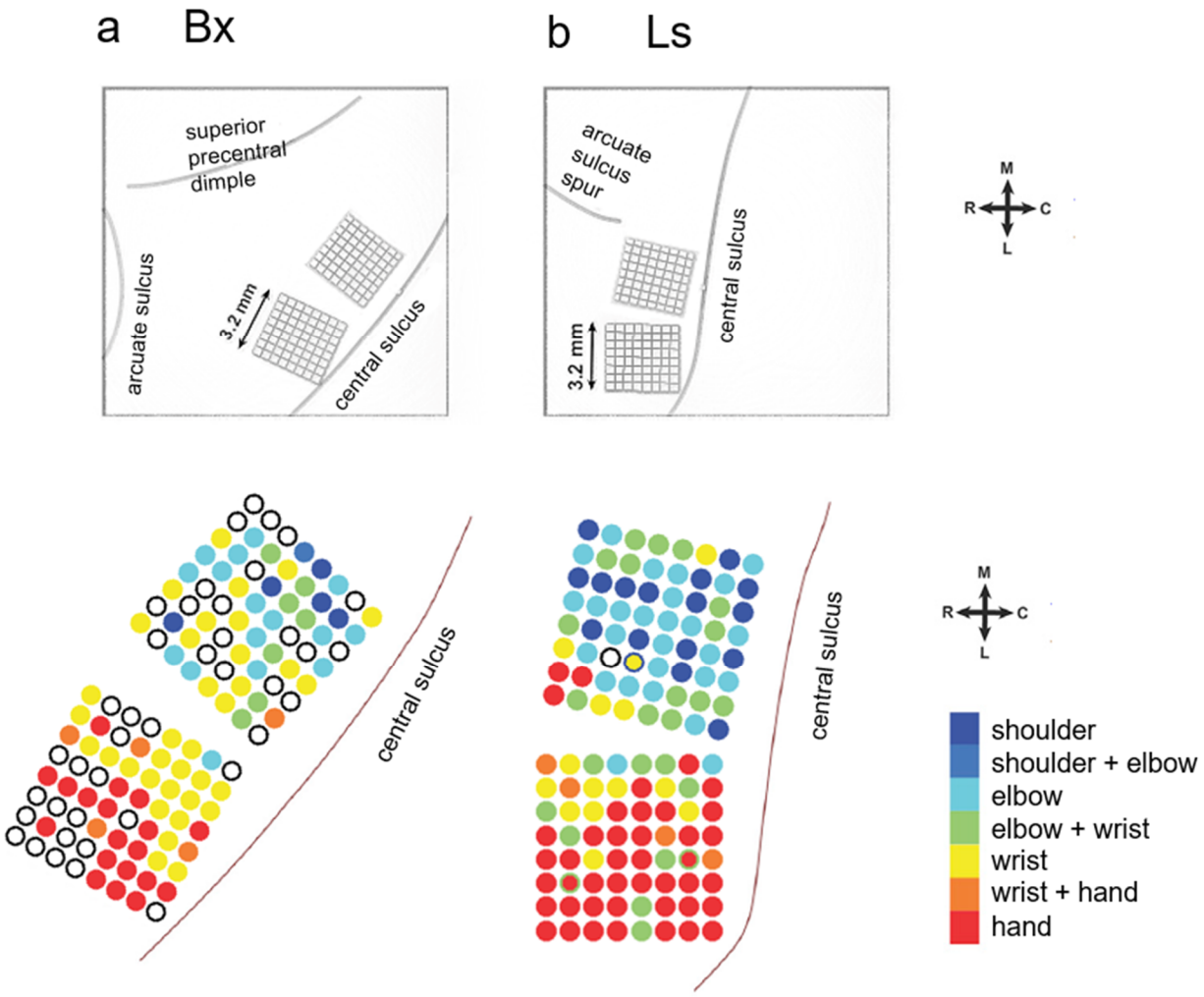

Fig. S1. Array implant locations and somatotopy. **a** & **b** are for Monkey Bx and Ls respectively. Top: two 8-by-8 Utah arrays were implanted in the primary motor cortex for each monkey. Bottom: somatotopic maps were obtained through suprathreshold intra-cortical microstimulation. Colors represent twitches on different body parts evoked during stimulation at the site, where mixed representations were illustrated as single intermediate colors (in cases of twitches of adjacent body parts) or different inner + outer colors (in cases of activations of non-adjacent body parts). Empty circles denote absence of observed twitches.

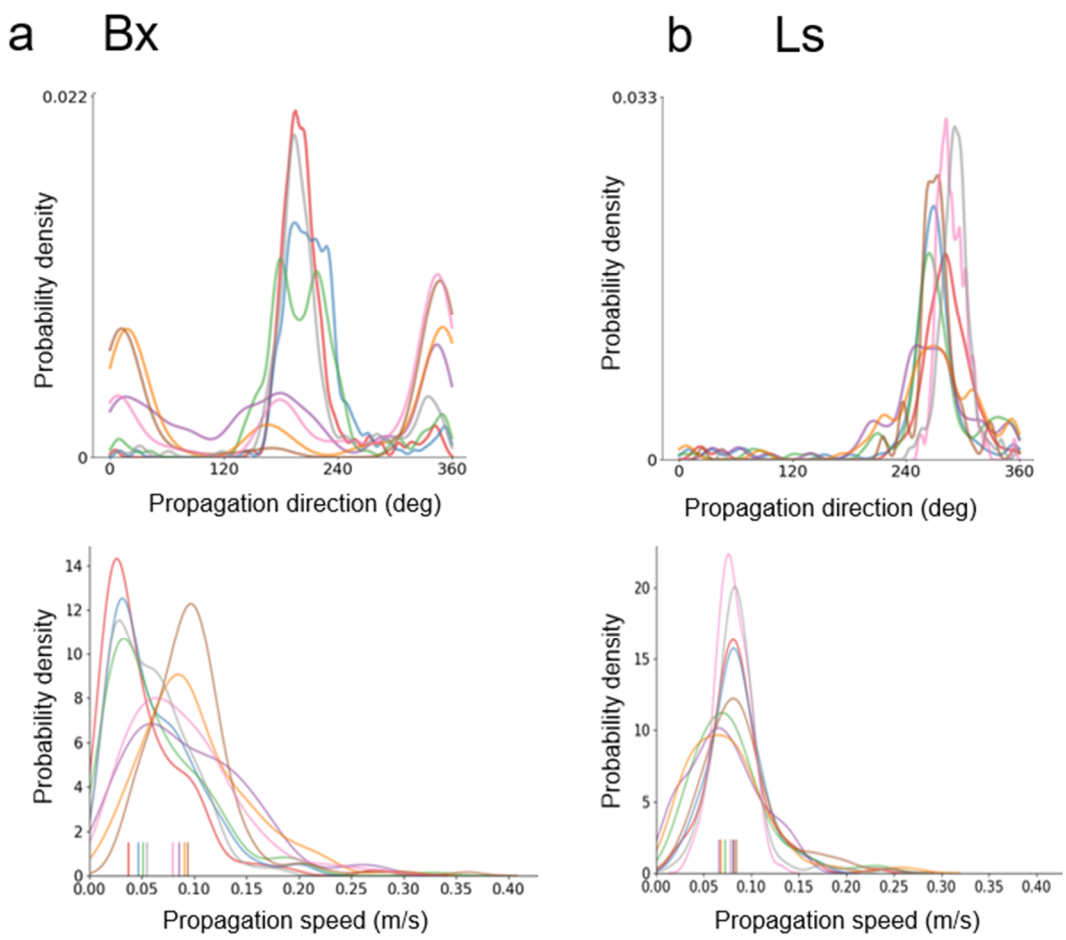

Fig. S2. Distributions of propagation properties for the lateral arrays. **a** & **b** are for monkeys Bx and Ls respectively. Colors represent target directions. Top: distribution of propagation directions for each target direction. Bottom: distribution of propagation speeds for each target direction (ticks represent median propagation speeds for individual target directions).

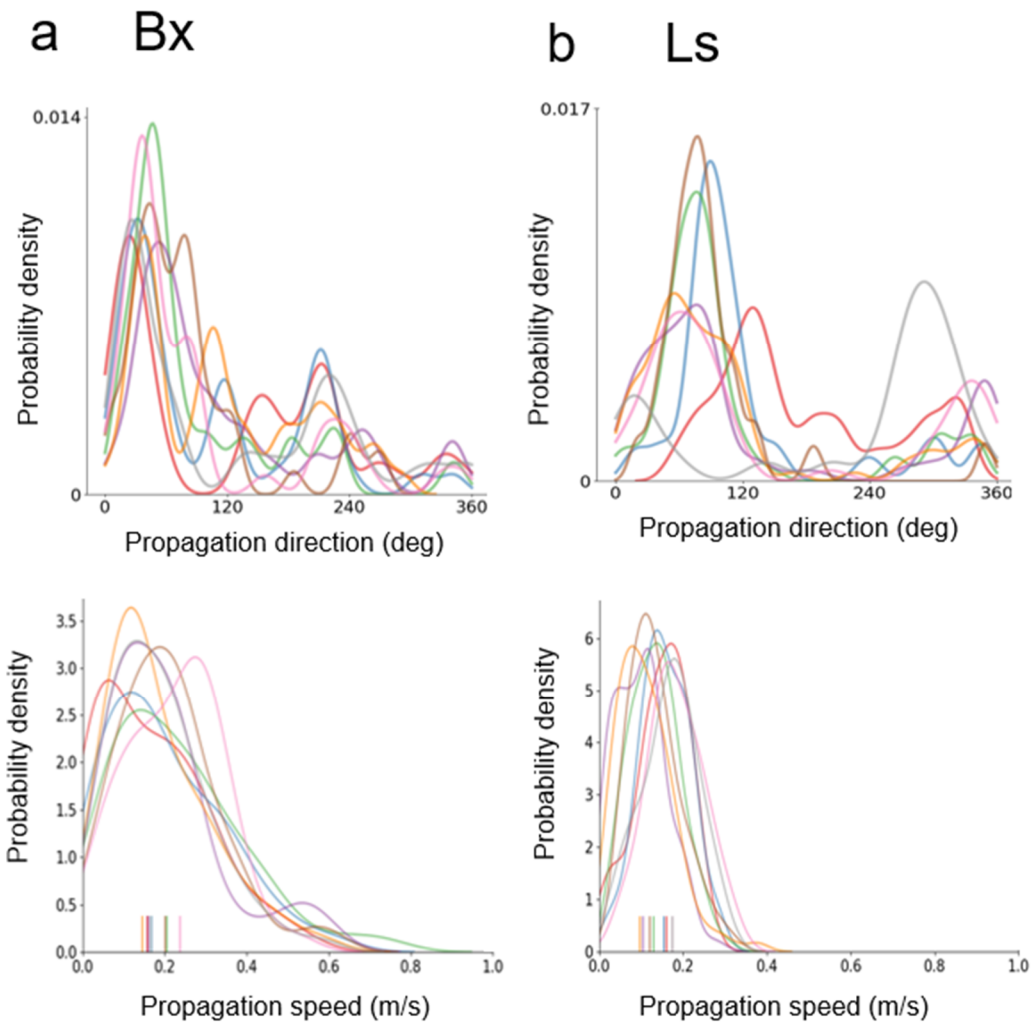

Fig. S3. Distributions of propagation properties for the medial arrays. **a** & **b** are for monkeys Bx and Ls respectively. Colors represent target directions. Top: distribution of propagation directions for each target direction. Bottom: distribution of propagation speeds for each target direction (ticks represent median propagation speeds for individual target directions).

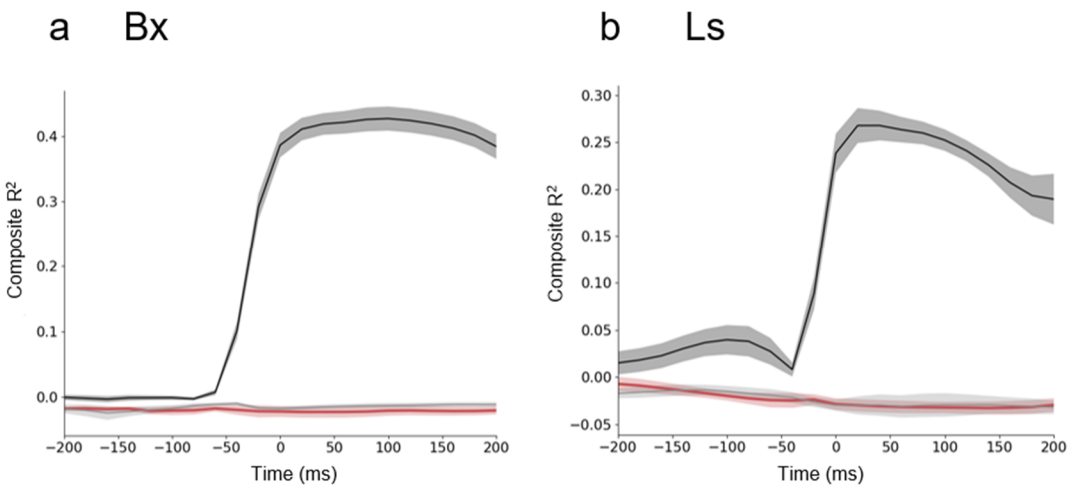

Fig. S4. Propagation parameters in the beta band cannot predict movement velocities. **a** & **b** are for monkeys Bx and Ls respectively. Red traces denote prediction performance (composite R^2) for hand velocities at different time points (w.r.t. movement onset) using all propagation parameters (i.e. propagation direction, speed and planar fitness from both arrays) in the beta band, which is indistinguishable from the gray traces denoting the performance from the trial-shuffled control. For reference, black traces represent the decoding performance from high-gamma band from **Fig. 6**. Error shade denotes sem from 10 folds.

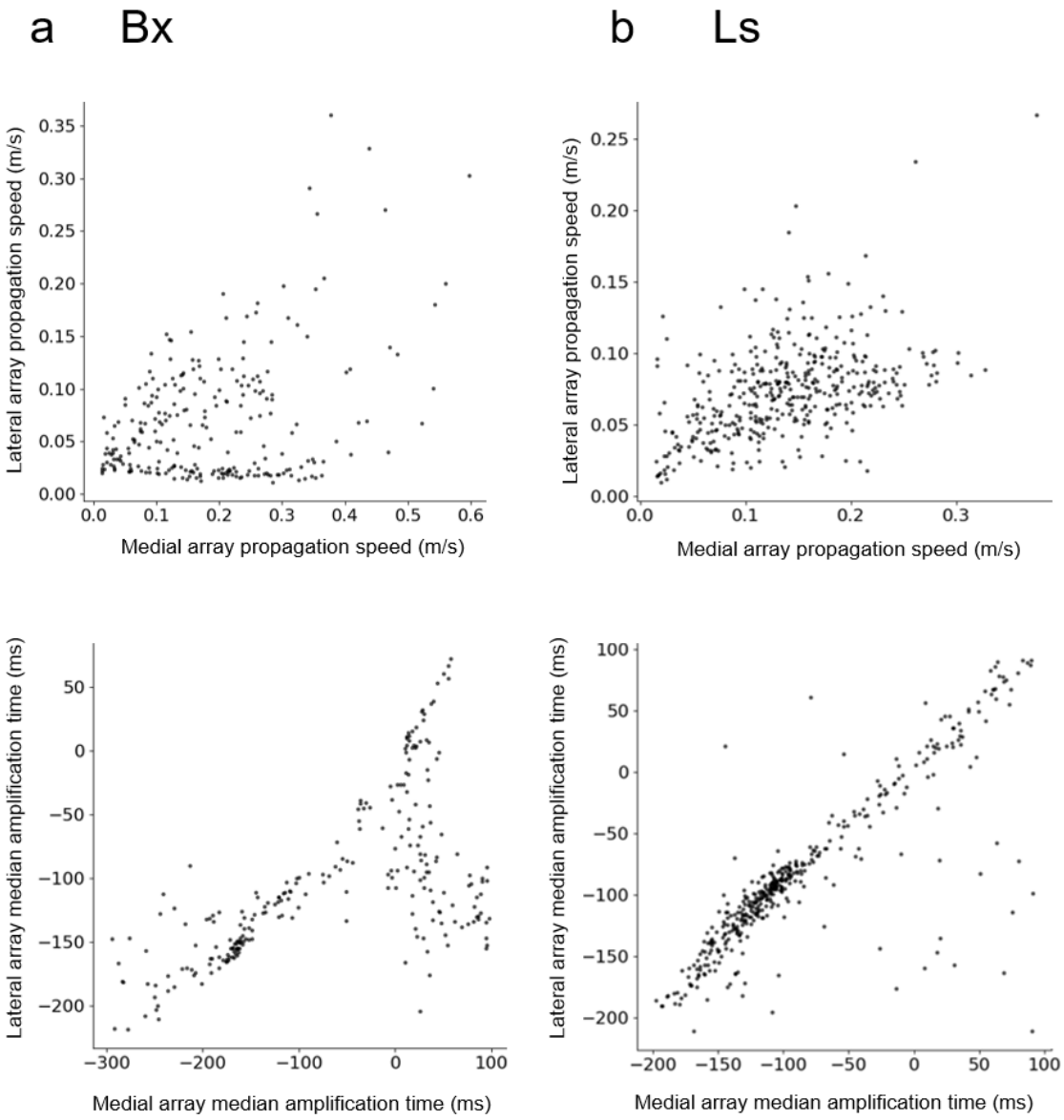

Fig. S5. Propagation patterns of the medial and lateral array were correlated on a trial-by-trial basis. **a** & **b** are for monkeys Bx and Ls respectively. Top: Scatter plots of the propagation speeds from the medial and lateral arrays for trials with significant propagation on both arrays, showing positive correlation between the two arrays (for Bx, $r=0.377$, $p<0.001$, $n=248$; for Ls, $r=0.473$, $p<0.001$, $n=415$; Pearson correlations test). Bottom: Scatter plots of the median amplification times (w.r.t. movement onset) from the medial and lateral arrays for trials with significant propagation on both arrays, showing positive correlation between the two arrays (for Bx, $r=0.610$, $p<0.001$, $n=248$; for Ls, $r=0.838$, $p<0.001$, $n=415$; Pearson correlations test).

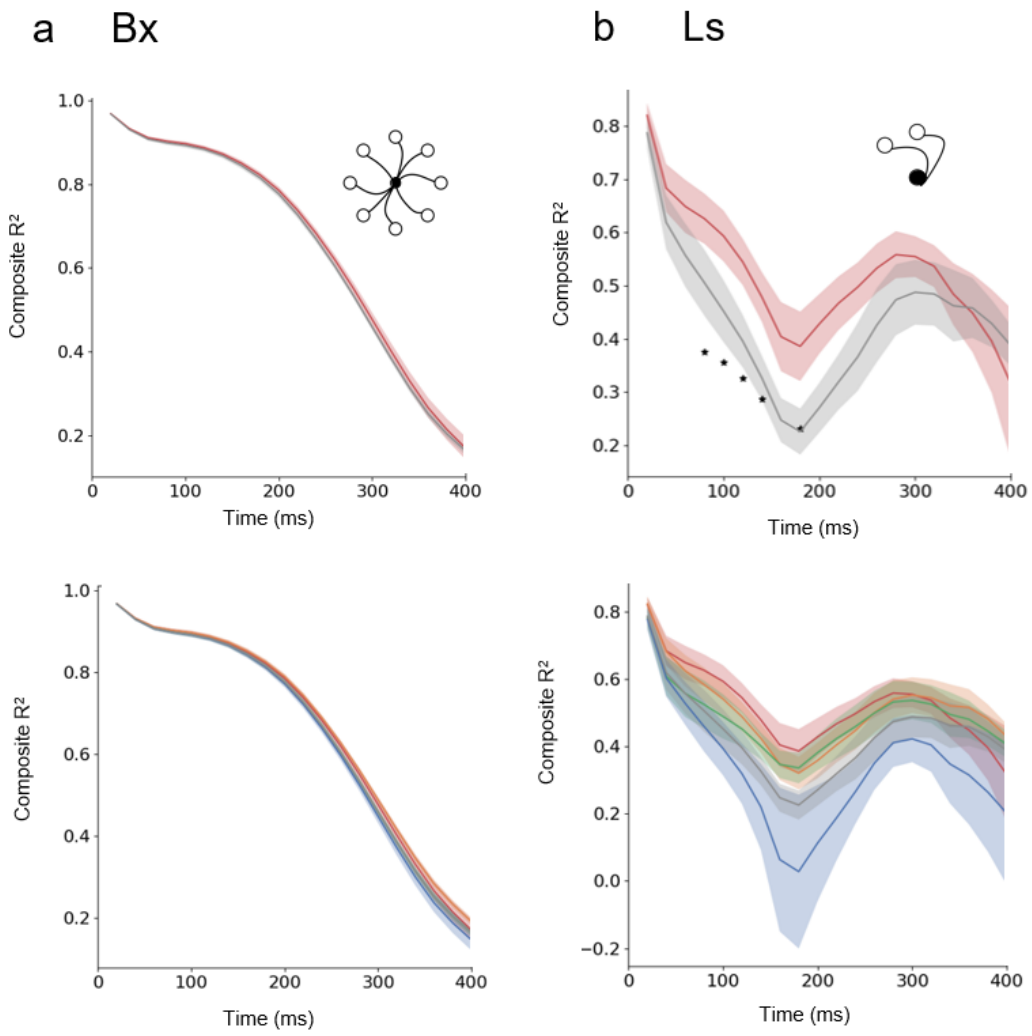

Fig. S6. Propagation parameters encoded for updating of hand velocities when trajectories were bent. a & b are for Monkey Bx and Ls respectively. Top: Prediction performance (composite R^2) for hand velocities at different time points (w.r.t. movement onset) using all propagation parameters (i.e. propagation direction, speed and planar fitness from both arrays) and launch velocities (red traces); gray line represents prediction performance (composite R^2) for hand velocities at different time points using launch velocities only. Error shade represents sem from 10 folds. Stars indicate that propagation parameters can predict kinematics significantly better than using launch velocities at the time points from single-tailed Wilcoxon test, Bonferroni-corrected for multiple comparisons. Insets show the mean trajectories to targets that were used in this prediction. For Bx, trials from all targets were used; for Ls, only trials from the two targets with bent trajectories were used. Bottom: breakdown of contributions from individual propagation parameters on hand velocity prediction. Red trace - all parameters as above, including launch velocities; orange trace – propagation direction and launch velocity; green trace – planar fitness and launch velocity; blue – propagation speed and launch velocity; gray — launch velocity only. For Ls, the added performance from high-gamma spatial variables primarily came from propagation direction and planar fitness.

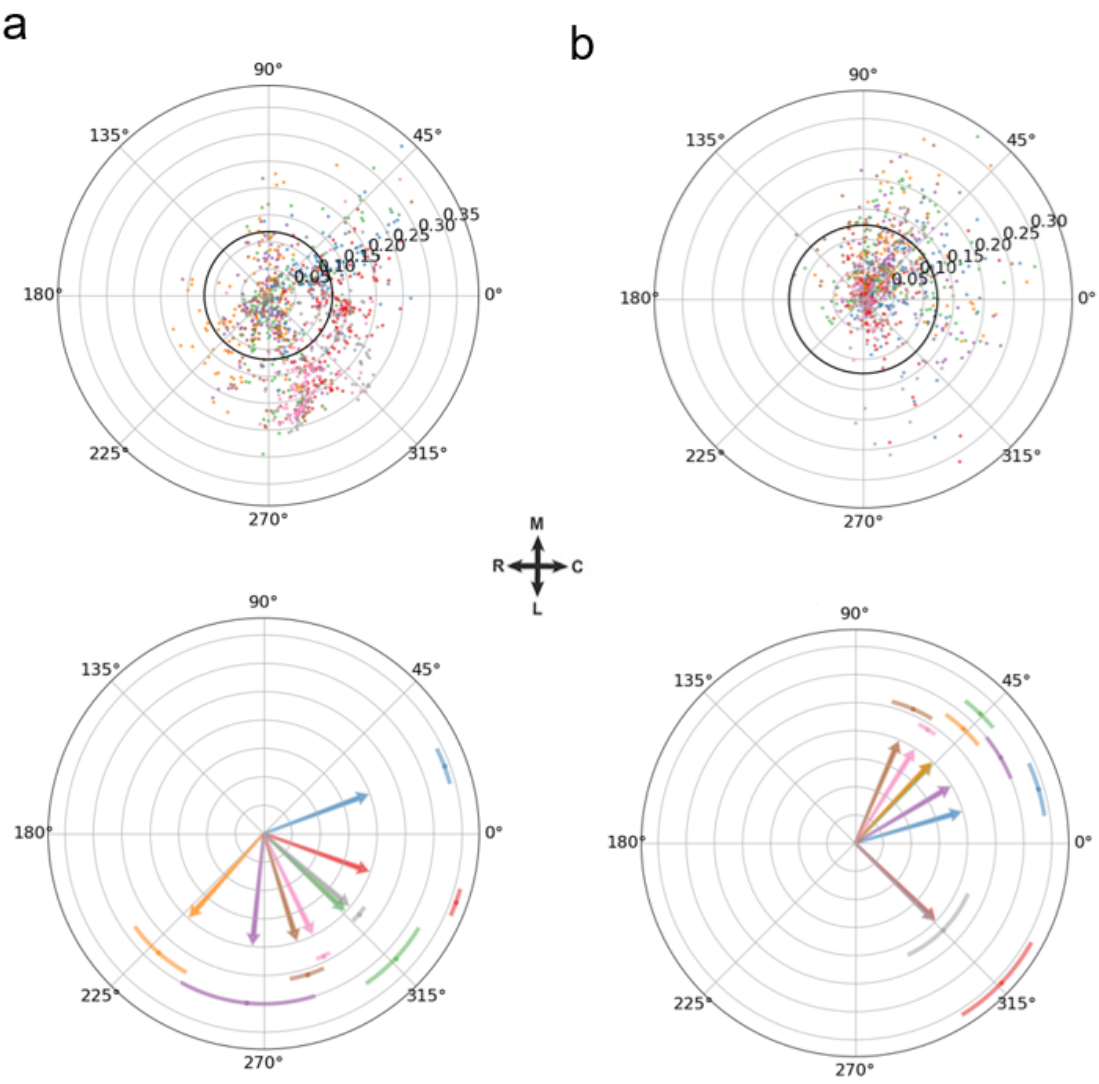

Fig. S7. Summary of MUA-based single-trial spatio-temporal propagation directions for Ls. **a** & **b** are for the lateral array and the medial array respectively. Top: polar scatter plot of propagation directions. Each dot is a single trial color-coded by reach direction. Angle represents propagation direction, while radius represents the associated R^2. Black solid circle represents the threshold of significant R^2 values. Bottom: summary of propagation directions for significant trials for each reach direction. Angle of arrow represents the mean propagation direction, while the error bar represents the 68.27% confidence interval for the mean.

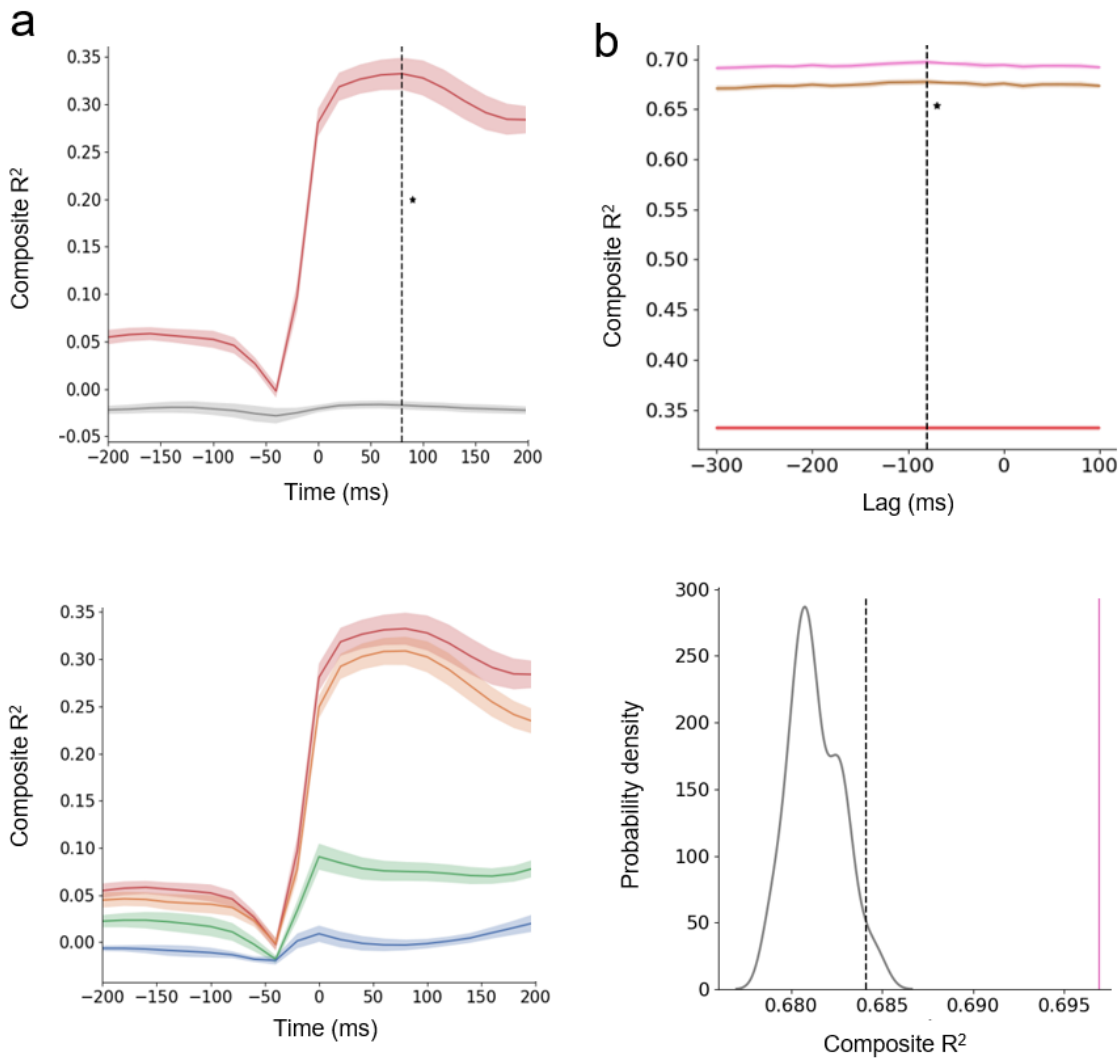

Fig. S8. MUA propagation parameters in Ls can be used to decode hand velocities and provided additional decoding performance on top of firing rates. **a**. Top: Prediction performance (composite R^2) for hand velocities at different time points (w.r.t. movement onset) using all MUA propagation parameters (i.e. propagation direction, speed and planar fitness from both arrays, all were 1st order). Red traces represent actual performance and gray line represents performance from the trial-shuffled control. Error shade represents sem from 10 folds. Optimal time where velocity prediction achieves best results is marked with the dotted vertical line (80ms w.r.t. movement onset). Star denotes that propagation parameters could predict kinematics significantly better than chance at the optimal time point from single-tailed Wilcoxon test. **a**. Bottom: breakdown of contributions from individual MUA propagation parameters on hand velocity prediction. Red trace - all parameters as above; orange trace – propagation direction only; green trace – planar fitness only; blue – propagation speed only. MUA propagation direction was more useful than propagation speed when used alone to predict movement velocities. **b.** Top: prediction performance (composite R^2) for hand velocities at different lags from the instantaneous amplitude envelope (negative lags means neural signals precede hand velocity), where brown trace denotes using instantaneous MUA firing rate only as predictors; red trace denotes using MUA propagation parameters only (1st and 2nd orders) as predictors (performance was lag-independent as there was only one set of spatial variables for the whole trial); pink trace denotes using both instantaneous MUA firing rate and MUA propagation parameters as predictors. Propagation

parameters here include not only 1st order parameters, but also 2nd order interactions terms. Error shade denotes sem from 10 folds. The time lag where the best mean envelope-amplitude-only performance was achieved was marked by the dotted vertical line (-80ms). Star denotes that MUA firing rate + propagation (pink) achieves significantly better prediction than firing rate-only (brown) at the best lag using a single-tailed Wilcoxon test. **b.** Bottom: the improved performance from including the MUA propagation parameters together with the MUA firing rate could not be obtained by merely adding propagation parameters from a random trial. The gray distribution shows the decoding performances of random additions of MUA propagation parameters from other trials together with the correct envelopes, with the top 5% threshold marked in dotted vertical black line. The solid pink vertical line denotes the real performance (i.e. addition of corresponding propagation parameters), which exceeds the dotted black line.

Table S1. MUA Propagation characteristics of trials with significant planar propagation on the lateral array for monkey Ls. sem is standard error of mean. r is length of the mean resultant vector of angles, which is a measure of concentration.

Reach target (deg)	Propagating direction (deg) (mean±sem) (r)	Propagating speed (m/s) (mean±sem) (median)	Sample size
0	316.6±11.6 (r=0.48)	0.057±0.009 (0.038)	48
45	20.5±5.0 (r=0.84)	0.045±0.005 (0.035)	60
90	340.3±3.4 (r=0.86)	0.056±0.004 (0.048)	119
135	319.8±3.3 (r=0.87)	0.052±0.002 (0.049)	123
180	295.9±2.3 (r=0.92)	0.052±0.002 (0.048)	117
225	287.2±6.1 (r=0.78)	0.050±0.006 (0.043)	51
270	228.2±11.9 (r=0.51)	0.049±0.008 (0.028)	39
315	264.2±5.6 (r=0.45)	0.044±0.009 (0.035)	15

Table S2. MUA Propagation characteristics of trials with significant planar propagation on the medial array for monkey Ls. sem is standard error of mean. r is length of the mean resultant vector of angles, which is a measure of concentration.

Reach target (deg)	Propagating direction (deg) (mean±sem) (r)	Propagating speed (m/s) (mean±sem) (median)	Sample size
0	46.1±5.5 (r=0.84)	0.035±0.002 (0.030)	50
45	16.4±7.6 (r=0.79)	0.045±0.004 (0.039)	31
90	316.2±13.8 (r=0.82)	0.047±0.010 (0.057)	9
135	315.5.6±19.4 (r=0.55)	0.046±0.009 (0.025)	13
180	57.7±3.4 (r=0.99)	0.069±0.005 (0.072)	5
225	66.8±7.8 (r=0.89)	0.059±0.018 (0.030)	21
270	46.7±7.4 (r=0.79)	0.036±0.003 (0.031)	33
315	30.7±7.5 (r=0.71)	0.046±0.003 (0.042)	43

Table S3. 100-200Hz Propagation characteristics of trials with significant planar propagation on the lateral array for monkey Bx. sem is standard error of mean. r is length of the mean resultant vector of angles, which is a measure of concentration.

Reach target (deg)	Propagating direction (deg) (mean±sem) (r)	Propagating speed (m/s) (mean±sem) (median)	Sample size
0	185.8±9.0 (r=0.36)	0.119±0.010 (0.084)	147
45	224.8±6.5 (r=0.40)	0.111±0.006 (0.088)	226
90	221.9±5.1 (r=0.50)	0.114±0.006 (0.092)	217
135	219.8±6.4 (r=0.44)	0.121±0.008 (0.094)	187
180	267.8±20.9 (r=0.18)	0.137±0.012 (0.109)	119
225	5.4±23.1 (r=0.16)	0.152±0.010 (0.128)	124
270	58.1±20.0 (r=0.18)	0.135±0.010 (0.106)	130
315	90.3±22.1 (r=0.17)	0.139±0.011 (0.105)	119

Table S4. 100-200Hz Propagation characteristics of trials with significant planar propagation on the lateral array for monkey Ls. sem is standard error of mean. r is length of the mean resultant vector of angles, which is a measure of concentration.

Reach target (deg)	Propagating direction (deg) (mean±sem) (r)	Propagating speed (m/s) (mean±sem) (median)	Sample size
0	291.4±7.9 (r=0.54)	0.080±0.006 (0.064)	76
45	273.6±5.3 (r=0.70)	0.102±0.007 (0.084)	92
90	294.4±4.1 (r=0.79)	0.098±0.004 (0.093)	105
135	291.6±3.3 (r=0.88)	0.093±0.005 (0.085)	118
180	287.1±2.5 (r=0.91)	0.088±0.004 (0.081)	111
225	290.0±7.6 (r=0.61)	0.090±0.006 (0.085)	64
270	306.4±13.7 (r=0.36)	0.095±0.010 (0.075)	66
315	319.9±13.2 (r=0.40)	0.094±0.009 (0.081)	55

Table S5. 100-200Hz Propagation characteristics of trials with significant planar propagation on the medial array for monkey Bx. sem is standard error of mean. r is length of the mean resultant vector of angles, which is a measure of concentration.

Reach target (deg)	Propagating direction (deg) (mean±sem) (r)	Propagating speed (m/s) (mean±sem) (median)	Sample size
0	231.3±11.9 (r=0.37)	0.327±0.025 (0.264)	82
45	No reliable mean or confidence interval due to low concentration (r=0.01)	0.343±0.024 (0.298)	80
90	185.2±42.3 (r=0.12)	0.333±0.022 (0.313)	77
135	No reliable mean or confidence interval due to low concentration (r=0.05)	0.320±0.024 (0.287)	63
180	259.1±16.9 (r=0.28)	0.313±0.023(0.290)	70
225	208.0±14.7 (r=0.27)	0.360±0.024 (0.299)	103
270	206.3±17.0 (r=0.32)	0.290±0.023 (0.251)	53
315	257.6±12.3 (r=0.38)	0.322±0.024 (0.239)	71

Table S6. 100-200Hz Propagation characteristics of trials with significant planar propagation on the medial array for monkey Ls. sem is standard error of mean. r is length of the mean resultant vector of angles, which is a measure of concentration.

Reach target (deg)	Propagating direction (deg) (mean±sem) (r)	Propagating speed (m/s) (mean±sem) (median)	Sample size
0	45.2±11.3 (r=0.43)	0.115±0.012 (0.097)	61
45	56.2±31.7 (r=0.19)	0.128±0.012 (0.123)	49
90	231.0±14.5 (r=0.35)	0.138±0.013 (0.120)	61
135	No reliable mean or confidence interval due to low concentration (r=0.07)	0.159±0.013 (0.139)	60
180	76.5±9.2 (r=0.68)	0.142±0.010 (0.138)	33
225	67.8±9.9 (r=0.53)	0.124±0.010 (0.116)	53
270	19.3±8.1 (r=0.58)	0.112±0.010 (0.100)	61
315	22.3±7.7 (r=0.57)	0.119±0.011 (0.107)	71